

## Amoeboid migration mode adaption in quasi-3D spatial density gradients of varying lattice geometry

This content has been downloaded from IOPscience. Please scroll down to see the full text.

2014 New J. Phys. 16 075012

(<http://iopscience.iop.org/1367-2630/16/7/075012>)

View [the table of contents for this issue](#), or go to the [journal homepage](#) for more

Download details:

IP Address: 132.229.211.17

This content was downloaded on 09/05/2017 at 12:34

Please note that [terms and conditions apply](#).

You may also be interested in:

[Collective cell migration: a physics perspective](#)

Vincent Hakim and Pascal Silberzan

[Collective cell motion in endothelial monolayers](#)

A Szabó, R Ünnepe, E Méhes et al.

[Invasion from a cell aggregate---the roles of active cell motion and mechanical equilibrium](#)

A Szabó, K Varga, T Garay et al.

[Mechano-sensing and cell migration](#)

C Borau, R D Kamm and J M García-Aznar

[Neutrophil adhesion and chemotaxis depend on substrate mechanics](#)

Risat A Jannat, Gregory P Robbins, Brendon G Ricart et al.

[A mechanical model for guided motion of mammalian cells](#)

P. Bitter, K. L. Beck and P. Lenz

[Collective cell streams in epithelial monolayers depend on cell adhesion](#)

András Czirók, Katalin Varga, Eld Méhes et al.

[The fundamental role of mechanical properties in the progression of cancer disease and inflammation](#)

Claudia Tanja Mierke

[Three-dimensional single-particle tracking in live cells: news from the third dimension](#)

A Dupont, M Gorelashvili, V Schüller et al.

## Amoeboid migration mode adaption in quasi-3D spatial density gradients of varying lattice geometry

Mari Gorelashvili<sup>1,3</sup>, Martin Emmert<sup>1,3</sup>, Kai F Hodeck<sup>1</sup> and Doris Heinrich<sup>1,2</sup>

<sup>1</sup>Fraunhofer Institute for Silicate Research ISC, Neunerplatz 2, D-97082 Würzburg, Germany

<sup>2</sup>Leiden University, LION Leiden Institute of Physics, Niels Bohrweg 2, 2333 CA Leiden, The Netherlands

E-mail: [doris.heinrich@isc.fraunhofer.de](mailto:doris.heinrich@isc.fraunhofer.de)

Received 15 March 2014, revised 15 May 2014

Accepted for publication 3 June 2014

Published 22 July 2014

*New Journal of Physics* **16** (2014) 075012

doi:[10.1088/1367-2630/16/7/075012](https://doi.org/10.1088/1367-2630/16/7/075012)

### Abstract


Cell migration processes are controlled by sensitive interaction with external cues such as topographic structures of the cell's environment. Here, we present systematically controlled assays to investigate the specific effects of spatial density and local geometry of topographic structure on amoeboid migration of *Dictyostelium discoideum* cells. This is realized by well-controlled fabrication of quasi-3D pillar fields exhibiting a systematic variation of inter-pillar distance and pillar lattice geometry. By time-resolved local mean-squared displacement analysis of amoeboid migration, we can extract motility parameters in order to elucidate the details of amoeboid migration mechanisms and consolidate them in a two-state contact-controlled motility model, distinguishing directed and random phases. Specifically, we find that directed pillar-to-pillar runs are found preferably in high pillar density regions, and cells in directed motion states sense pillars as attractive topographic stimuli. In contrast, cell motion in random probing states is inhibited by high pillar density, where pillars act as obstacles for cell motion. In a gradient spatial density, these mechanisms lead to topographic guidance of cells, with a general trend towards a regime of inter-pillar spacing close to the cell diameter. In locally anisotropic pillar environments, cell migration is often found to be damped due to competing attraction by different pillars in close proximity and due to lack of other potential stimuli in the vicinity

<sup>3</sup> These authors contributed equally to this work.



Content from this work may be used under the terms of the [Creative Commons Attribution 3.0 licence](https://creativecommons.org/licenses/by/3.0/). Any further distribution of this work must maintain attribution to the author(s) and the title of the work, journal citation and DOI.

of the cell. Further, we demonstrate topographic cell guidance reflecting the lattice geometry of the quasi-3D environment by distinct preferences in migration direction. Our findings allow to specifically control amoeboid cell migration by purely topographic effects and thus, to induce active cell guidance. These tools hold prospects for medical applications like improved wound treatment, or invasion assays for immune cells.

 Online supplementary data available from [stacks.iop.org/NJP/16/075012/mmedia](http://stacks.iop.org/NJP/16/075012/mmedia)

Keywords: amoeboid migration, topographic guidance, 3D environmental structure, cell motility, cell migration assay

## Introduction

Amoeboid motion is a particularly efficient form of cell migration, characteristic for several cell types, e.g. stem cells, specific immune cells or metastatic tumor cells. In the human body, these cell types exhibit rapid migration through diverse types of tissue, enabling them to travel long distances to their point of destination [1].

The high efficiency of amoeboid migration is the result of interplay of fast cytoskeletal dynamics and relatively weak, short-lived contacts to the substrate [2–8]. These mechanisms allow for a rapid response to chemical and mechanical cues in the cells' environment [9]. For example, amoeboid migration is observed for neutrophils and leukocytes, migrating towards the source of an inflammation in response to molecular signaling cascades [10]. Interestingly, similar signaling cascades and corresponding response mechanisms can be observed in *Dictyostelium discoideum* (Dd) amoebae [11]. Thus, Dd is both a biologically relevant and experimentally robust model organism to study amoeboid cell migration as a response to environmental cues [12].

Influence on cell migration can be generated by several types of external cues like chemical signals [13–18] and mechanical stimuli [19–21]. Topographic variations in the vicinity of migrating cells are a special type of mechanical stimulus, but their importance becomes clear by looking at human tissue: cells are always facing local variations in their natural environment, as the local topography inside tissue of the human body is far from being isotropic. In fact, tissue is the antipode of the flat and smooth glass substrates commonly used in 2D *in vitro* migration assays. Recent progress in technologies for controlled fabrication of micro- and nano-structures facilitated the investigation of cell behavior in response to topographic variations like grooves or pillars. However, extensive studies on cell orientation [22, 23] and migration [24, 25] led to sometimes contradictory findings, even for the same substrate structures and cell types [26, 27]. In this context, it is crucial to establish model experimental situations to control and measure the effects of topographic stimuli on migrating cells precisely and reproducibly. By that, more detailed numerical analyses enable reliable interpretations and predictions with respect to realistic 3D conditions inside the human body.

Following this approach, we designed systematically controlled assays to assess the influence of topographic cues on cell migration behavior. In particular, we used PDMS micro-pillar fields consisting of lattices of trigonal (isotropic) and hexagonal/honeycomb (anisotropic)

geometry with defined density gradients, providing spatially controlled quasi-3D environments for cell migration. In doing so, we take advantage of the fact that PDMS is a comprehensively characterized standard material, which provides a well-controllable model environment for systematic cell migration studies [29, 32]. To exclude surface-induced or chemically related side-effects, the pillar samples were produced from bulk material, exhibiting uniform surface structure and chemical composition. This way, we make sure that the pillars and the bottom in between them are of the same material. For all experiments the pillars are non-flexible posts of the same diameter  $d = 4 \mu\text{m}$ . This way, changes in the migration behavior of cells in contact with the pillar structures can be related solely to the topographic properties of the environment. By performing local mean squared displacement (l-MSD) analysis of cell trajectories within the pillar fields we extract cell motility parameters from phases of directed runs (dir-runs) and random motion modes (rm-modes) of amoeboid migration. This allows us to analyze changes in cell migration behavior with respect to local variations in pillar density and pillar lattice structure. First, we study the effect of the spatial pillar density on Dd single cells migrating in quasi-3D micro-pillar fields of varying pillar densities. As a second part of this work, we investigate the influence of the local geometry on cell migration by comparison of Dd migration in trigonal (isotropic) and hexagonal (anisotropic) pillar fields. Finally, we examine topography-induced cell guidance effects in dependence on pillar density gradients and lattice geometry.

With this study, we aim at revealing the mechanisms governing amoeboid cell migration by structural cues in a quasi-3D environment. A detailed understanding of these mechanisms will allow for topographic control of amoeboid cell migration, holding prospects for future applications, e.g. for the design of invasion assays for immune cells and smart materials for wound treatment.

## Materials and methods

Amoeboid migration of single *D. discoideum* (Dd) cells in the vegetative state was studied. The experiments were performed at low cell density in the absence of cell nutrients, in order to avoid external chemical stimuli biasing cell migration. We observed Dd cells in quasi-3D environments, provided by hexagonal arrays of micro-pillars, fabricated from transparent polydimethylsiloxane (PDMS). For systematic study of cell migration in response to topographic cues, we varied the inter-pillar distance and the geometry of the pillar arrays in a controlled manner. PDMS as a material is stiff (elastic modulus  $E = 1.72 \text{ MPa}$  [32]) with respect to the relatively weak adhesion forces exhibited by Dd cells [33, 34]. This allows for the investigation of structural determinants of amoeboid cell migration independent of the details of the particular cell–substrate interaction. Fluorescently labeled Dd cells and transparent PDMS pillar arrays were imaged by fluorescence and bright-field microscopy. Cell migration analysis was performed by using an established cell tracking routine [30] and l-MSD analysis software [28].

## Cell culture and microscopy imaging

### *Cell culture*

The axenic Dd strain (HG1694) expressing freeGFP (obtained from Dr Günther Gerisch, MPI for Biochemistry, Martinsried, Germany) was grown in HL5 medium (ForMedium™,

Hunstanton, UK) adjusted at pH=6.7 and complemented by the antibiotic Gentamycin at a concentration of  $20 \mu\text{g mL}^{-1}$  (G-418, Biochrom AG, Berlin, Germany). The cell confluence was kept below 40%.

For microscopy experiments, HL5 medium was substituted by phosphate buffered saline (PBS), adjusted at pH=6.0. The cell–PBS suspension was filled into the observation chamber (composed of a cover glass and a Teflon<sup>®</sup> frame) and rested for 20 min to let the cells settle down, until a concentration of 10–20 cells per  $400 \times 400 \mu\text{m}^2$  (camera field of view) was achieved.

### *Microscopy*

The measurements were carried out with a 20× objective (Nikon, Germany) on a Nikon Eclipse Ti microscope (Nikon, Germany) equipped with an EM-CCD camera (Hamamatsu, Herrsching, Germany) at 19–21 °C. Fluorescence and bright field images of fluorescently labeled cells and transparent pillar arrays were acquired every 10 s for at least one hour to exclude short-time effects. To minimize the excitation stress for the cells, exposure times were kept below 100 ms.

### **Preparation of micron-sized PDMS pillar structures**

Substrates on which cells were seeded were made out of the transparent polymer polydimethylsiloxane (PDMS), after its casting, cross-linking and unpeeling from a silicon wafer-based master obtained by standard photolithography procedures. The PDMS structures resulting from this process were two different types of arrays of 10–12  $\mu\text{m}$  high pillars with a constant diameter of 4  $\mu\text{m}$ .

Experimental characterization by scanning electron microscopy shows that the pillars are in fact highly uniform, with variations in dimension on nanometer scale, due to the precisely controlled fabrication process of the samples (see supporting information, available from [stacks.iop.org/NJP/16/075012/mmedia](http://stacks.iop.org/NJP/16/075012/mmedia), figure S1). The PDMS micro-pillar array fabrication was done by the standard procedure previously described by Steinberg *et al* [29]. The well-defined character, i.e. constant diameter, of the PDMS micro-pillars used for our cell migration experiments has already been demonstrated by Arcizet *et al* [31]. Accordingly, variations in stiffness of the pillars influencing the cell interaction can be excluded for the experiments.

Pillars were arranged in (i) arrays of trigonal geometry with gradients in lattice constant, ranging from 8.2  $\mu\text{m}$  to 22.5  $\mu\text{m}$ , or in (ii) lattices of hexagons with gradients in hexagon side length ranging from 10.5  $\mu\text{m}$  to 38.4  $\mu\text{m}$ . Please note that all substrates, including the micro-pillars and the areas in between, exhibit the same chemical composition. This way any external chemical bias of cell migration can be excluded.

### *Master fabrication*

Master fabrication was performed by standard clean room microlithography procedures, according to protocols described by Steinberg *et al* [29]. Therefore, a 3 inch silicon wafer (Si-Mat, Landsberg/Lech, Germany) was cleaned under nitrogen flow protection and covered with 5 ml of SU8-10 negative photoresist (Microchem, distributed by Micro Resist Technology, Berlin, Germany) by spin-coating at 3000 rpm for 30 s. After that, the substrate was progressively soft-baked (1 min at 65 °C and 2 min at 85–90 °C, cooling down slowly to room

temperature) and illuminated with UV-light in a mask aligner (Süss MicroTec, Garching, Germany) through a chromium mask (ML&C, Jena, Germany), with varying illumination times of 3–5 s, according to the intended structure sizes. The illumination was followed by a progressive hard bake of 1 min at 65 °C, and 2 min at 85–90 °C, with cooling down slowly to room temperature. After that, the unilluminated photoresist was removed by two bathing steps in SU8-specific developer (MicroResist Technology, Berlin, Germany).

### *Preparation of the PDMS structures*

The resist master was silanized by vapor deposition of fluorosilane (1H,1H,2H,2H-perfluorooctyltrichlorosilane, ABCR, Germany) under vacuum for one hour. The PDMS base and the cross-linking agent were mixed at a 1 : 10 ratio (Sylgard 184 Silicone Elastomer Kit, Dow Corning, MI, USA) and degassed for 30 min under vacuum. Subsequently 2–3 ml of PDMS was poured on the Si-photoresist master, and degassed again for 15–30 min under vacuum. PDMS cross-linking was obtained after 3–5 h at 65 °C. After cutting and peeling the PDMS structures off the master, the samples were immediately transferred to the observation chambers (consisting of a cover glass and a Teflon<sup>®</sup> frame), immersed in PBS solution and stored until use for cell migration experiments.

### **Cell migration analysis**

Cell migration analysis was performed in two steps. First, center of mass positions ( $X$  and  $Y$  coordinates) of each cell, investigated at each time point of the experiment, were obtained from fluorescence images using a cell tracking plug-in [30] for ImageJ image analysis software (W S Rasband, US National Institutes of Health, Bethesda, USA, <http://imagej.nih.gov/ij/>). This plug-in detects cells as clusters of more than  $n$  bright pixels of a certain set intensity  $I$  in closer proximity than a distance  $d$ . All of these parameters were adjusted optimally for precise cell recognition.

In a second step, the obtained cell position data were processed using a homemade Matlab algorithm. This algorithm was adapted from the previously developed TRAnSpORT routine [28, 31] and is able to distinguish two modes of cell migration—directed runs and random motion phases—in a time-resolved manner. For this purpose, TRAnSpORT routine uses global as well as l-MSD analysis of cell trajectories.

Instantaneous migration velocity and direction are obtained from the changing positions of the center of mass of the cell. A global trend towards a migration state of a more ‘diffusive’ or a more ‘directed’ character is determined by global MSD (MSD) analysis over the entire trajectory of each cell.

The l-MSD analysis is based on a two-state model of cell migration, extracting alternate phases of directed runs and diffusive-like random walks [7, 31]. The directed parts of the trajectory correspond to phases when the amoeba crawls at a quasi-constant speed in a quasi-constant direction. The directed runs are separated by non-directed phases, during which the cell probes its environment, repolarizes and starts a new directed run in another direction. As a key feature, the l-MSD analysis algorithm is capable of distinguishing the two motility modes in the migration trajectories. After trajectory splitting, the phase durations can be retrieved, together with specific migration parameters, such as velocity for the directed runs, and a diffusion coefficient analogue for the random motion states. The power of this method lies within the fact



that the parameters are evaluated only during the corresponding phases of the motion. This prevents, for example, phases of directed motion from biasing the overall statistical analysis by increasing the global diffusion coefficient analogue. Moreover, the local analysis reveals otherwise hidden features of the migration behavior, which are related to local or short-term stimuli.

l-MSD  $\Delta R_i^2(\tau_k)$  and angle persistence  $\Delta\varphi_i(t_i, \tau_k)$  are calculated over a rolling window of  $M=30$  frames for each experiment time point  $t_i$  of the trajectory as a function of different lag times  $\tau_k = k \cdot \delta t$  as follows:

$$\begin{aligned} \Delta R^2(t_i, \tau_k) &= \Delta R_i^2(\tau_k) \\ &= \frac{1}{M - k + 1} \sum_{j=-M/2}^{M/2-k} \left( \mathbf{R}(t_{i+j} + \tau_k) - \mathbf{R}(t_{i+j}) \right)^2 \end{aligned} \quad (1)$$

$$\begin{aligned} \Delta\varphi(t_i, \tau_k) &= \Delta\varphi_i(\tau_k) \\ &= \sqrt{\frac{1}{M - k + 1} \sum_{j=-M/2}^{M/2-k} \left( \varphi(t_{i+j} + \tau_k) - \varphi(t_{i+j}) \right)^2}. \end{aligned} \quad (2)$$

Here,  $\mathbf{R}(t_i) = (X(t_i), Y(t_i))$  is the coordinate of the center of mass of the cell and  $\delta t = 10$  s is the inverse frame rate of the experiment. In previous work, the l-MSD analysis algorithm was tested with the precisely controlled motion of latex beads in microfluidic stop-flow experiments [28]. Based on this calibration, the window size is adapted for application to biophysical questions. In this context, we showed that the temporal resolution obtained by the l-MSD analysis is of the order  $\frac{M \cdot \delta t}{4}$  s [28]. Specifically for cell migration in PDMS pillar fields we determined  $M=30$  frames per time point as suitable window size [31], which is chosen accordingly for the comparable experimental setting in this work. The l-MSD function is fitted by using a well-established relation from statistical physics:

$$\Delta R^2(t_i, \tau_k) = A \cdot \tau_k^\alpha.$$

Here, the exponent  $\alpha$  characterizes the migration state of the cell and the prefactor  $A$  bears either the information about the diffusion coefficient analogue of random diffusive-like migration modes or the velocity of directed runs. For  $\alpha \approx 2$  and a persistent angle of motion, the cell migration state is defined as ‘directed’, otherwise as ‘random’ migration mode. The l-MSD algorithm defines the probability for directed motion for a certain time point as

$$P_{\text{dir}} = \begin{cases} 1 & \text{for } [1.7 \leq \alpha \leq 2] \wedge [0 \leq \Delta\varphi \leq 0.9 \text{ rad}] \\ 0 & \text{otherwise} \end{cases}$$

Further, phase durations  $\tau^{\text{rm}}$  and  $\tau^{\text{dir}}$  for random states and dir-runs are computed, as well as the overall probability  $P^{\text{rm}}$  and  $P^{\text{dir}}$  for each migration mode.

## Results and discussion

In this work, we study the influence of structural properties of the local environment on amoeboid migration of Dd cells in the vegetative state, in the absence of any chemical

attractors. Specifically, we investigate the influence of spatial density and geometry of the environment, independently of the details of the particular substrate adhesion mechanism of the cells. Therefore, we analyze amoeboid cell migration within well-defined micro-pillar arrays of gradient inter-pillar distance and different lattice geometry. Standard pillars of  $4\ \mu\text{m}$  diameter and  $10\text{--}12\ \mu\text{m}$  height are made of polydimethylsiloxane (PDMS) by standard photolithography and polymer molding procedures. To avoid chemically related side effects, the entire substrate was fabricated from bulk material exhibiting homogeneous chemical composition and surface properties. Please note that within the pillar arrays, the cells migrate in a quasi-3D environment, i.e. on the bottom substrate in between the pillars, not on top of pillars. Migration of fluorescently labeled Dd cells in transparent PDMS pillar arrays is imaged by fluorescent and bright field microscopy.

We analyze first the migration of cells in fields of trigonal lattice structure and different pillar density. For our investigations, we measured cells in pillar arrays of gradient inter-pillar distance ranging from values close to half the average cell size (diameter) up to twice the cell size. Accordingly, we differentiate between three regions of spatial density of the pillar fields: (i) low density regions, where cells contact only one to two pillars simultaneously, (ii) intermediate density regions, where cells sense three to five pillars in their immediate vicinity and (iii) high density regions, where the cells are squeezed in between more than five neighboring pillars. Secondly, we study the effect of geometry by comparison between cell migration in isotropic trigonal (T-arrays) (figures 2(A)–(C)) and in anisotropic hexagonal lattices (H-arrays) of gradient inter-pillar distance. Hexagonal arrays are congruent with trigonal lattices, where the pillar in the center of each hexagon is missing (figures 3(A)–(C)). Thus, H-arrays lack the local topographic isotropy exhibited by T-arrays. Further, hexagonal lattices provide more space for cell migration on the ‘floor’ (base substrate) in between pillars compared to trigonal pillar arrays. Thirdly, we analyze guidance of cells by topographic cues, specifically with respect to the direction of the pillar density gradient and the respective lattice vectors of the pillar arrays.

For data evaluation, center of mass trajectories of cells within pillar arrays were extracted from the obtained image stacks. A typical cell trajectory in a trigonal pillar array for a time period of 68 min is shown in figure 1(A). The obtained data were analyzed with respect to cell migration [7, 31]. MSD lag-time dependent analysis of the whole cell trajectory bears information on global migration properties of different time-scales, as illustrated by figure 1(B). Here, a distinct decrease in the exponent  $\alpha$  for increasing lag-times is shown. To resolve the migration state of the cell at each experiment time point, we perform l-MSD analysis within a predefined time window (of length  $M=30$  frames), sliding along the entire cell trajectory. By that, each cell trajectory is divided into phases of directed runs (dir-runs) and random motion (rm-mode), as shown in figure 1(C). This analysis is based on the lag-time dependent l-MSD function as shown in figure 1(D), which bears the full information of all states for each time point. During directed runs (dir-runs), a cell migrates at nearly constant velocity and exhibits a high directional persistence. In random migration phases, cells probe their environment in a diffusive-like manner without any preferred migration direction. The migration state is identified as dir-run by criterion of the l-MSD exponent  $\alpha \approx 2$  and angular persistence  $\Delta\varphi \approx 0$ , or is assigned the rm-mode in all other cases. The numerical analysis of the cell motility states yields distributions for the l-MSD exponent  $\alpha$ , for instantaneous velocities  $v^{\text{rm}}$  and  $v^{\text{dir}}$  and for phase durations  $\tau^{\text{rm}}$  and  $\tau^{\text{dir}}$ , as well as the



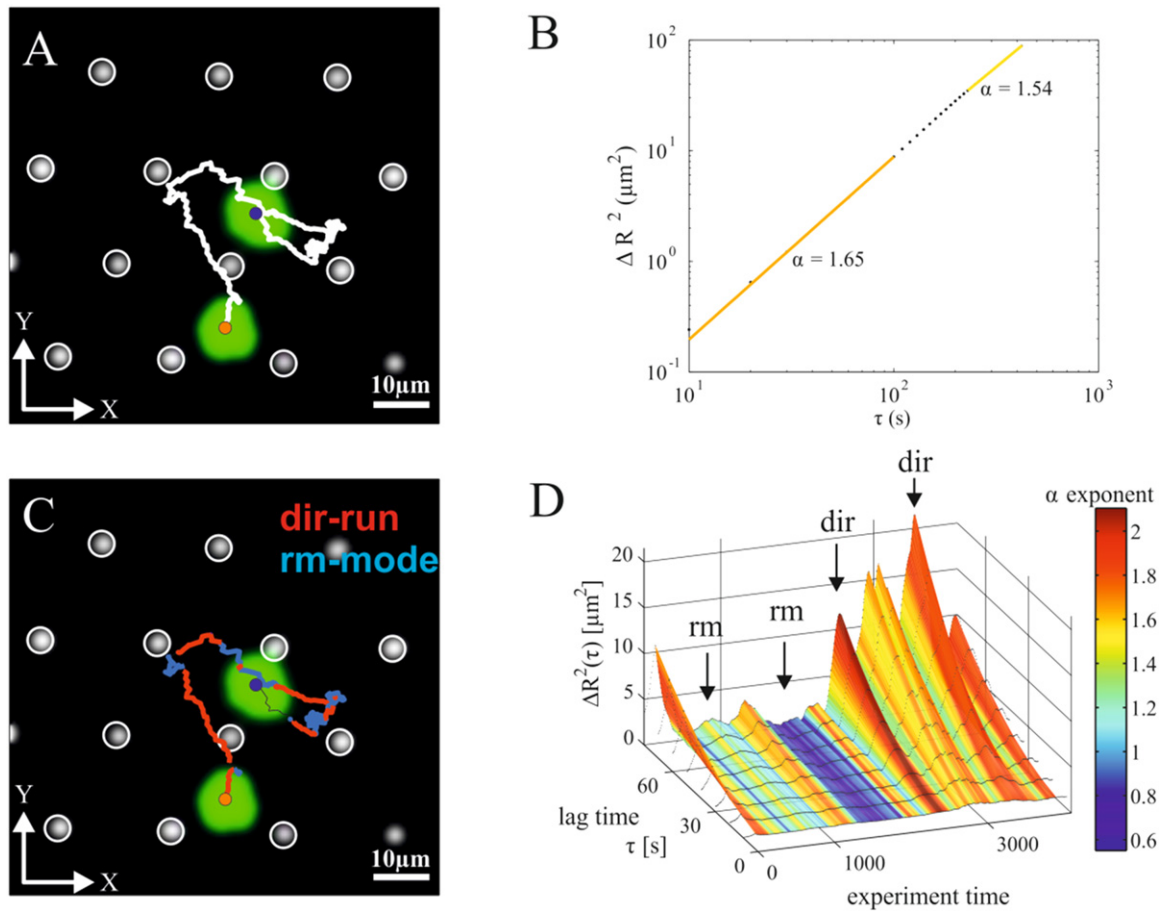


**Figure 1.** Two-state amoeboid motility model. (A) Typical trajectory (white curve) of a *D. discoideum* amoeba cell (green) migrating in a quasi-3D trigonal pillar lattice (white pillar tops). White circles highlight positions of the pillars, which are of uniform shape and constant diameter of  $4\ \mu\text{m}$ . The cell is shown for time points  $t_1 = 0$  min and  $t_2 = 68.2$  min, with corresponding positions of its center of mass in blue ( $t_1$ ) and orange ( $t_2$ ). (B) Global mean squared (MSD) analysis of the cell trajectory in (A), revealing different motility state trends, by change of slope as a function of the lag-time  $\tau$ . (C) Cell trajectory of (A) split into directed runs (dir-run) of almost constant velocity and high directional persistence (red), and random migration phases (rm-mode) (blue), using local MSD analysis. (D) Landscape-plot of the local MSD function, bearing information of lag-time dependent motility states for each time point of the experiment. The local MSD exponents, which quantitatively describe the motility state, are color-coded, whereby dir-runs are shown in red and rm-modes in yellow to blue, depending on the value of the exponent.

overall probabilities  $P^{\text{rm}}$  and  $P^{\text{dir}}$  to be in the rm-state or to perform a dir-run, which are discussed at first by evaluation of their mean values. Further, the numerical distributions of the cell migration parameters were statistically characterized by their median values and the measures for deviation and relative asymmetry, as listed in table S1. We find that in all pillar arrays, cell migration can be well characterized by the two-state motility model and cells exhibit dir-runs as well as rm-modes.

## Cell migration in isotropic trigonal pillar arrays of varying lattice constant

To study the influence of pillar density on cell motion, we analyze cell migration ( $N=126$  cells,  $n=44\,200$  data points) within micro-pillar arrays of regular trigonal lattice structure exhibiting a density gradient. With respect to the mean cell size, we define three regimes of the pillar lattice constant  $a$  as  $a > 16\,\mu\text{m}$  (region T1),  $16\,\mu\text{m} > a > 13\,\mu\text{m}$  (region T2) and  $13\,\mu\text{m} > a$  (region T3), representing low, intermediate and high pillar density, respectively. In comparison, the typical cell size (diameter) of Dd amoeba is  $\sim 8\text{--}12\,\mu\text{m}$ . Figures 2(A)–(C) show representative images of cells in pillar fields of trigonal lattice geometry at low (T1), intermediate (T2) and high density (T3). Please note that figures 2(A)–(C) show genuine microscopy images which have been optimized for acquisition of the fluorescent cells' positions in the quasi-3D environments of not fluorescently labeled pillar fields. This explains the slightly different image appearance of the pillars, which are in fact highly uniform, with a diameter of  $4\,\mu\text{m}$  and extremely small variation in dimension (see figure S1). For Dd cells the pillars act as uniform, non-flexible posts they encounter in their migration paths.

In the low density regime (T1), cells can attach to one or two pillars at the same time (figure 2(A)), but are able to sense more neighboring pillars by filopodia. In the intermediate regime (T2), cells can establish contacts with three to five pillars simultaneously (figure 2(B)). For a high pillar density, cells are squeezed in between more than five pillars (figure 2(C)).

### High pillar density facilitates dir-runs

Local-MSD analysis of cell motility states (i.e. directed runs and random migration modes) in different density regimes of the trigonal pillar lattices reveals a distinct dependence of amoeboid cell migration on spatial density. The probability for dir-runs shows the highest value at high pillar density ( $P_{T3}^{\text{dir}} = 25.1\%$ ), followed by the low density regime ( $P_{T1}^{\text{dir}} = 20.4\%$ ), while it is significantly lower at intermediate pillar density ( $P_{T2}^{\text{dir}} = 16.2\%$ , for reference: on flat PDMS substrate  $P_{2D}^{\text{dir}} = 35\%$ ) (table 1). In addition, the values of angular persistence  $\Delta\varphi$  are slightly higher for high and low density regimes than for intermediate spatial density of T-arrays (figures 2(J)–(L) and table 1). The mean value of the l-MSD exponent  $\langle\alpha_T^{\text{dir}}\rangle$  of the dir-run states is nearly equal for all density regimes of trigonal pillar arrays and for 2D substrates (figures 2(D)–(F), table 1). These results reveal that dir-runs are more pronounced in high and low density regions of the trigonal arrays, as compared to intermediate density areas.

Analysis of the instantaneous velocities during directed migration phases reveals a positive correlation with the spatial pillar density, with respective mean values  $v_{T1}^{\text{dir}} = 0.033\,\mu\text{m s}^{-1}$ ,  $v_{T2}^{\text{dir}} = 0.036\,\mu\text{m s}^{-1}$  and  $v_{T3}^{\text{dir}} = 0.043\,\mu\text{m s}^{-1}$  (figures 2(G)–(I)). Further, the persistence times of the dir-run modes show a peak in the high density regime (T3), with a mean value of  $\tau_{T3}^{\text{dir}} = 131.6\text{ s}$ . The corresponding distribution of the dir-run phase durations is broadened and shifted to higher values, compared to the low density (T1) and the intermediate regime (T2). Phase duration distributions of the complementary rm-modes reveal that these phases are shortened in the high density regime (T3) (figures S2 (A)–(C)). In contrast, in the low density regime (T1), the persistence times of the random

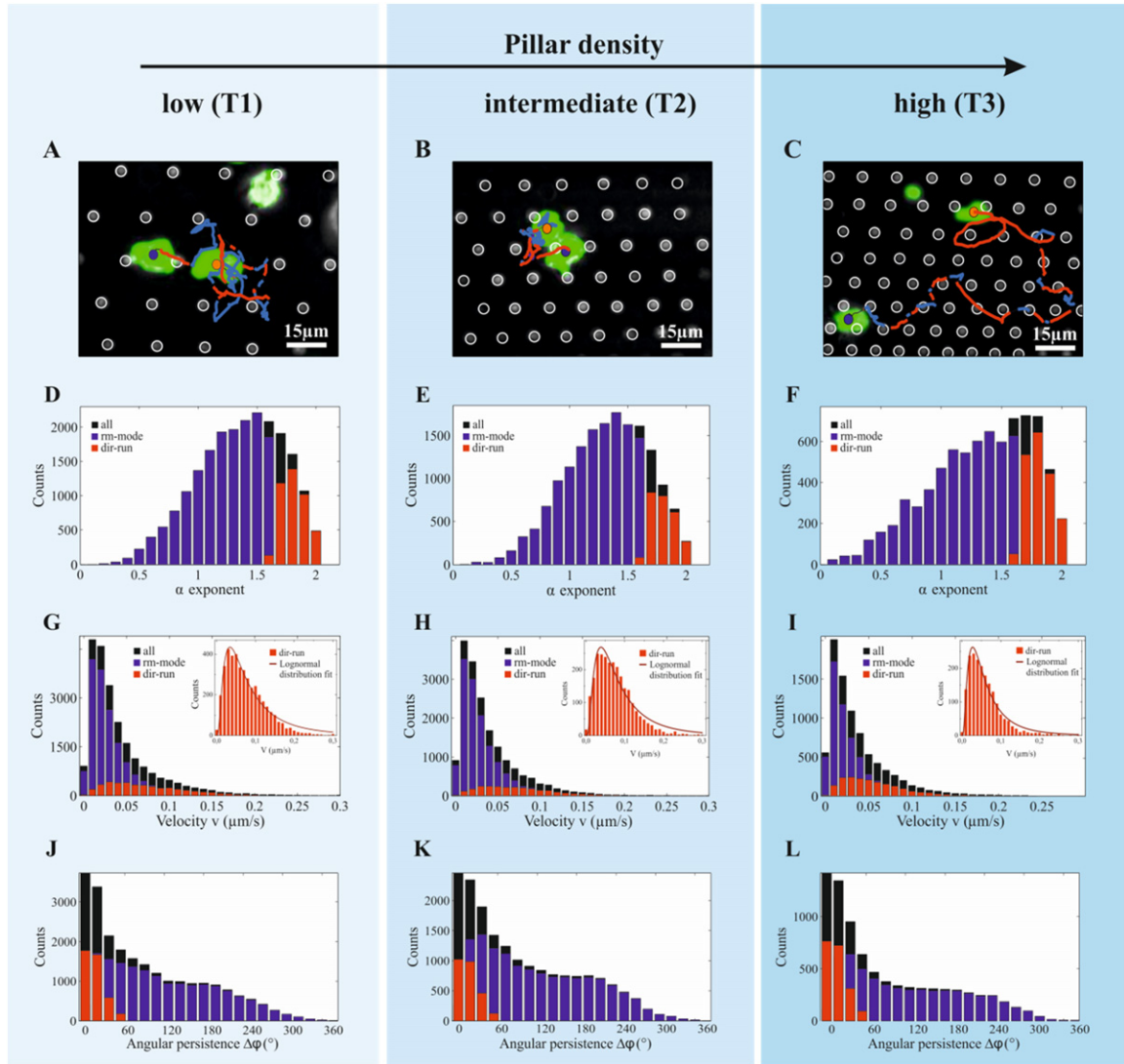


**Figure 2.** Cell migration in trigonal lattices of varying pillar density regimes. Cell motility state characteristics for cells migrating in isotropic trigonal pillar lattices of low (T1), intermediate (T2) and high density (T3). (A), (B), (C) Typical trajectories of *D. discoideum* cells (green), with phases of directed runs (red) and random migration modes (blue). Cells are shown for time points  $t_1 = 0$  min and  $t_2 = 50$  min (A),  $t_2 = 53$  min (B) and  $t_2 = 90$  min (C), respectively. The corresponding cell center of mass positions are highlighted in blue ( $t_1$ ) and orange ( $t_2$ ). White circles highlight positions of the pillars, which are of uniform shape and constant diameter of  $4\ \mu\text{m}$ . (D), (E), (F) Distributions of alpha exponents of dir-runs (red), rm-modes (blue) and all values (black) describing the characteristics of cell motion in the different pillar density regimes. (G), (H), (I) Corresponding distributions of instantaneous velocities during dir-runs (red) and rm-modes (blue). The overall distributions of instantaneous velocities are shown in black. Insets show velocity distributions of dir-runs, fitted by log-normal distribution function. (J), (K), (L) Angular persistence of cell migration during directed runs (red) and random migration modes (blue). The overall distribution is shown in black.

**Table 1.** Parameters describing cell motility in pillar lattices of trigonal (T1, T2, T3) and hexagonal (H1, H2, H3) lattice geometry and different inter-pillar distances, corresponding to figures 2 and 3. For reference, cell migration data on flat PDMS substrate are shown (2D) [31].

		T1	T2	T3	H1	H2	H3	2D
		$a > 16 \mu\text{m}$	$16 \mu\text{m} > a > 13 \mu\text{m}$	$13 \mu\text{m} > a$	$r > 16 \mu\text{m}$	$16 \mu\text{m} > r > 10 \mu\text{m}$	$10 \mu\text{m} > r$	
Number of data points in the statistics	$N$	20 663	15 998	7539	14 402	5794	7504	12 338
Exponents of the 1-MSD power law								
Directed runs	$\alpha^{\text{dir}}$	1.81	1.81	1.81	1.78	1.76	1.80	1.81
Random migration states	$\alpha^{\text{rm}}$	1.22	1.21	1.15	1.18	1.17	1.13	1.30
Diffusion coefficient analog ( $\mu\text{m}^2 \text{s}^{-1}$ )	$D$	0.0090	0.0078	0.0084	0.0068	0.0066	0.0075	0.0072
Instantaneous velocity ( $\mu\text{m} \text{s}^{-1}$ )								
Directed runs	$V^{\text{dir}}$	0.033	0.036	0.043	0.069	0.053	0.046	0.075
Random migration states	$V^{\text{rm}}$	0.032	0.030	0.028	0.029	0.028	0.027	0.044
Lifetimes of states (s)								
Directed runs	$\tau^{\text{dir}}$	119.2	108.0	131.6	91.1	71.5	100.3	155
Random migration states	$\tau^{\text{rm}}$	302.2	371.6	286.8	424.7	513.9	555.8	238.7
Angular persistence (deg)								
Directed runs	$\Delta\phi^{\text{dir}}$	14.67	15.83	15.53	17.82	18.85	17.02	16.51
Random migration states	$\Delta\phi^{\text{rm}}$	115.59	116.25	120.31	126.25	127.57	124.84	89.91
Dir-num probability	$P^{\text{dir}}$	20.4	16.2	25.1	8.8	6.4	9.4	35
Random mode probability	$P^{\text{rm}}$	79.6	83.8	74.9	91.2	93.6	90.6	65

modes are longer. Compared to trigonal lattices, on flat PDMS substrate cells performing dir-runs exhibit higher migration velocities and larger values for temporal persistence  $\tau$ , while the temporal persistence of rm-modes is lowered (table 1 and table S1).

Together, these results indicate that in the trigonal pillar lattice, the high density regime (T3) facilitates directed cell runs in terms of high velocities and persistence times, as well as increased probability. The enhancement of the dir-run mode by the high density regime supports the concept of pillars acting as topographic ‘attractors’ to the cells, as introduced by Arcizet *et al* [31]. During directed migration phases, cells show contact-controlled motility and perform pillar-to-pillar runs. While coming into contact with one pillar, a cell simultaneously senses its environment and can start a dir-run to the next pillar, found in its immediate vicinity. At lower pillar densities, cells exhibit a decreased probability of sensing neighboring pillars and thus, dir-runs are less frequent with a smaller mean phase duration, as compared to the high density regions (T3) (see supplementary data, movie S1). In conclusion, cells in the dir-run migration state sense pillars as topographic stimuli and orient their motion towards them, performing contact-controlled pillar-to-pillar runs.

#### *Random motion—pillars act as obstacles*

In contrast to dir-run states, we find that during random migration (rm) phases the pillars act as obstacles for cell motion. The quantitative analysis of the rm-states reveals a negative correlation of the exponent  $\alpha_T^{\text{rm}}$  and of the motion velocity  $v_T^{\text{rm}}$  with the spatial density of the pillar arrays. While the distributions and the mean values of  $\alpha_T^{\text{rm}}$  exponents are similar for low (T1) and intermediate (T2) density areas, the mean value is lower for dense regions (T3) ( $\alpha_{T1}^{\text{rm}} \approx \alpha_{T2}^{\text{rm}} \approx 1.21$ ,  $\alpha_{T3}^{\text{rm}} = 1.15$ , for reference  $\alpha_{2D}^{\text{rm}} = 1.30$ ). The distribution of the exponents  $\alpha_T^{\text{rm}}$  broadens for the high density region (T3) (compared to (T1) and (T2)), where extremely low values are reached for a large number of data points (figures 2(D)–(F) and table S1). A similar trend can be observed for the mean values of migration velocities  $v_T^{\text{rm}}$  (see table 1). The distribution of the velocities  $v_{T3}^{\text{rm}}$  shows a distinct shift to lower values compared to less dense pillar regions. Correspondingly, the mean value of angular persistence of cell migration in random mode significantly increases for the high density regime T3 compared to T1 and T2 arrays (figures 2(J)–(L) and table 1). Also, the probability for rm-states for high density (T3) areas  $P_{T3}^{\text{rm}} = 74.9\%$  is significantly lower than the respective probabilities  $P_{T1}^{\text{rm}} = 79.6\%$  for low density (T1) areas and intermediate density (T2) areas ( $P_{T2}^{\text{rm}} = 83.8\%$ ). In addition, the diffusion coefficient analogue decreases for high density areas (T3), compared to (T1) ( $D_{T3} = 0.0084 \mu\text{m}^2 \text{ s}^{-1}$  and  $D_{T1} = 0.0090 \mu\text{m}^2 \text{ s}^{-1}$ ). Compared to cell migration on flat substrates, in trigonal lattices the probability for rm-modes as well as the mean velocity in this migration state is lowered and the angular persistence of cell motion is significantly reduced (table 1). Taken together, these results reflect the ‘diffusion-like’ character of random probing migration phases, analogue to a passive drift of particles in crowded media: While at high pillar densities the probability for rm-states is reduced in general, the increase in the crowdedness of the environment dampens the particular random motion processes and thus lowers the  $\alpha_T^{\text{rm}}$  exponent values, as well as the diffusion coefficient analogue  $D_T$  (see figure S3). Accordingly, during rm-modes, pillars act as obstacles for cell motion.

### *Cell trapping at intermediate density regime in isotropic pillar lattice structure*

Another important observation is the reduced probability of performing dir-runs for cells migrating in the intermediate density (T2) areas of the trigonal pillar lattices, as compared to the regions of low (T1) and high (T3) pillar density. Here, the inter-pillar distance is in the regime of the typical diameter of Dd cells, so that cells are often attached to several pillars simultaneously. In this constellation, a cell displaces its center of mass back and forth from one pillar to the other (figure 2(B)). In terms of l-MSD analysis, these cell events are classified as rm-modes, exhibiting low values of the diffusion coefficient analogue, as compared to the migration phases of cells on flat surfaces, which are not ‘caged’ by topographic cues. Due to this phenomenon, the mean value of diffusion coefficient analogue  $D_T$  reaches its minimum, and the mean duration of rm-modes  $\tau_T^{\text{rm}}$  reaches its maximal value in the intermediate density (T2) region. On the other hand, the probability  $P_T^{\text{dir}}$  and the exponent  $\alpha_T^{\text{dir}}$  of the dir-runs show the lowest values in the intermediate regime (T2). Additionally, the mean persistence time of dir-runs is minimal in this region ( $\tau_{T2}^{\text{dir}} = 108.0$  s). The effect of cell trapping in intermediate density regimes originates from the cell ‘attachment’ to several pillars at the same time. In this constellation, a stable cell polarization to one particular direction is impeded, and the cell is temporarily trapped in between several pillars, as described in former work [31]. From such a ‘trapped’ state the cell can only escape by an occasional, strongly asymmetric repolarization, or sensing of distant pillars with exceptionally long protrusions.

### **Cell migration in micro-pillar hexagonal arrays of varying side length**

To investigate the influence of the local geometric structure of the quasi-3D environment on cell migration, we analyze cell trajectories in micro-pillar arrays of hexagonal lattice geometry (H-arrays) exhibiting a spatial density gradient. H-arrays are congruent with trigonal lattices, where the pillar at the center of each hexagon structure is missing, as shown by figures 3(A)–(C). Please consider that the microscopy images are tuned to track the position of the fluorescently labeled cells, thus hiding the high uniformity of the actual pillar dimensions.

In trigonal lattices, cells sense a topographically isotropic environment, i.e. the spatial distribution of surrounding pillars is independent of the cell position. By comparison, in the H-arrays the perceived geometry of the surroundings is anisotropic and depends on the position of the cell within the hexagon (honeycomb). In order to extract comparable pillar densities for the analysis of cell migration in hexagonal lattices as in the trigonal lattices, we redefine the three spatial density regimes as a function of hexagon side length  $r$  to  $r > 16 \mu\text{m}$  (H1),  $16 \mu\text{m} > r > 10 \mu\text{m}$  (H2), and  $10 \mu\text{m} > r$  (H3) representing low, intermediate and high pillar density in H-arrays, respectively. Again, the inter-pillar distance of intermediate (H2) density region is close to the mean diameter of a Dd cell, while in the low (H1) and in high (H3) density regions, it is comparable to half and to twice the size of these cells, respectively.

### *General pillar-density dependent cell migration mechanisms*

In hexagonal pillar lattices with gradients in inter-pillar distance (H-arrays), l-MSD analysis of cell trajectories ( $N=47$  cells,  $n=27\,700$  data points) yields analogue trends as for the cell migration behavior observed in trigonal pillar arrays (T-arrays). In detail, the probability for dir-runs  $P^{\text{dir}}$ , the local-MSD exponents  $\alpha^{\text{dir}}$  and  $\alpha^{\text{rm}}$ , as well as the persistence of dir-modes  $\tau^{\text{dir}}$  and



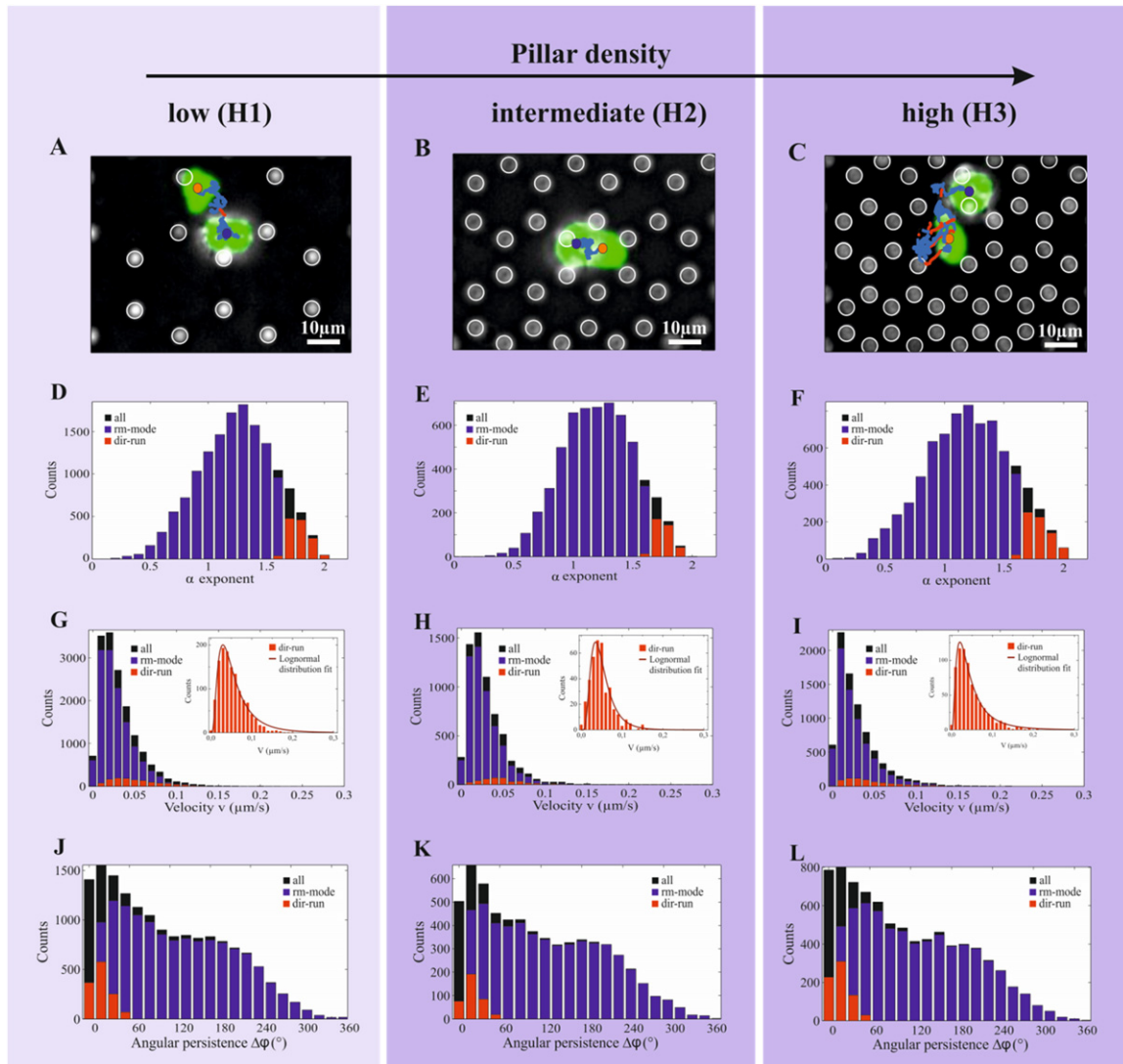


**Figure 3.** Cell migration in hexagonal lattices of varying pillar density regimes. Cell motility state characteristics for cells migrating in anisotropic hexagonal pillar lattices of low (H1), intermediate (H2) and high density (H3). (A), (B), (C) Typical trajectories of *D. discoideum* cells (green), with phases of directed run states and random probing highlighted in red and blue, respectively. Cells are shown for time points  $t_1 = 0$  min and  $t_2 = 83$  min, with corresponding center of mass positions in blue ( $t_1$ ) and orange ( $t_2$ ). White circles highlight positions of the pillars, which are of uniform shape and constant diameter of  $4\ \mu\text{m}$ . (D), (E), (F) Distributions of alpha exponents of dir-runs (red), rm-modes (blue) and all values (black), describing the character of cell motion in different density regimes. (G), (H), (I) Corresponding distributions of instantaneous velocities during dir-runs (red) and rm-modes (blue). The overall distributions of instantaneous velocities are shown in black. Insets show velocity distributions of dir-runs, fitted by log-normal distribution function. (J), (K), (L) Angular persistence of cell migration during directed runs (red) and random migration modes (blue). The overall distributions are shown in black.

the mean instantaneous velocity during rm-modes  $v^{\text{rm}}$  exhibit analogue dependence on the pillar density in both types of pillar arrays (table 1). This result suggests that there are general mechanisms controlling cell migration by spatial density in the quasi-3D environment, independent of lattice geometry: contact-controlled pillar-to-pillar guidance during dir-runs and diffusive-like character of rm-modes appear in trigonal as well as in hexagonal arrays of gradient spatial density. In both lattices the migration states show similar dependence on the pillar density. For reference, table 1 shows respective migration parameters for cell migration in 2D [31]. Reduced probability of topography-induced cell migration confinement in high (H3) density regions leads to increased cell motility in this density regime. The corresponding mean value of  $D_H$  is 10–12% higher in high density (H3) regions compared to the low (H1) and intermediate density (H2) regions ( $D_{H1} = 0.0068 \mu\text{m s}^{-1}$ ,  $D_{H2} = 0.0066 \mu\text{m s}^{-1}$  and  $D_{H3} = 0.0075 \mu\text{m s}^{-1}$ ).

### *Influence of topographic anisotropy on cell migration*

However, there is also a strong difference in cell migration within the two lattice types. Notably, the absolute values of cell migration parameters are strongly affected by different lattice structures. In particular, the probabilities of dir-runs in H-arrays are less than half compared to T-arrays, and to flat substrates (see table 1). In addition, the distributions of the exponents  $\alpha_H^{\text{dir}}$  and  $\alpha_H^{\text{rm}}$  exhibit a shift to smaller values compared to the corresponding values of  $\alpha_T^{\text{dir}}$  and  $\alpha_T^{\text{rm}}$  (figures 3(D)–(F) and table 1). Further, the dir-runs in H-arrays are less persistent in terms of state duration and migration direction ( $\Delta\varphi$ ) than in trigonal pillar lattices. Specifically, the duration  $\tau^{\text{dir}}$  is reduced by 23–33% as compared to T-arrays (and by 36–54% as compared to flat substrates). The distinct suppression of dir-runs in H-arrays is related to the locally anisotropic structure of the cells' environment. Therefore, the trapping of cells in between several pillars as described above is more probable in hexagonal arrays than in trigonal lattices (see supplementary data, movie S3). Due to the absence of the pillars at the center of each hexagon, the probability for a cell to sense other pillars as topographic stimuli and escape from the trapped state is significantly lowered. Correspondingly, in H-arrays a strong increase in the mean duration of random probing modes  $\tau^{\text{rm}}$  is found. Compared to the respective values found for T-arrays, the values of  $\tau^{\text{rm}}$  are increased by  $\sim 40\%$  for low (H1) and intermediate (H2) regions and even 94% for the high (H3) density region (and by 78–132% as compared to 2D substrate) (table 1). Further, the values of the diffusion coefficient analogue  $D_H$  are decreased by 10–25% with respect to  $D_T$ . Thus, although in H-arrays cells can migrate in regions containing fewer obstacles than in the trigonal lattices, cells exhibit reduced motility in terms of the diffusion coefficient analogue  $D_H$ .

Another interesting observation concerning the hexagonal lattices is the overall increase in instantaneous velocities of the dir-runs, as compared to T-arrays, in spite of the reduced probability and mean duration of dir-runs. This means that in H-arrays the rare pillar-to-pillar runs are performed at velocities  $v_H^{\text{dir}}$  higher than  $v_T^{\text{dir}}$  (but still lower than  $v_{2D}^{\text{dir}}$ ). This effect can be explained by the absence of center pillars in the hexagons: As the cells sense less topographic stimuli sideways while migrating in dir-run mode, they continue their runs with less disturbance and change of direction.

In summary, we find local anisotropy of lattice structure in H-arrays strongly influences cell migration, leading to a more complex variety of behavior, compared to our findings in isotropic trigonal arrays.

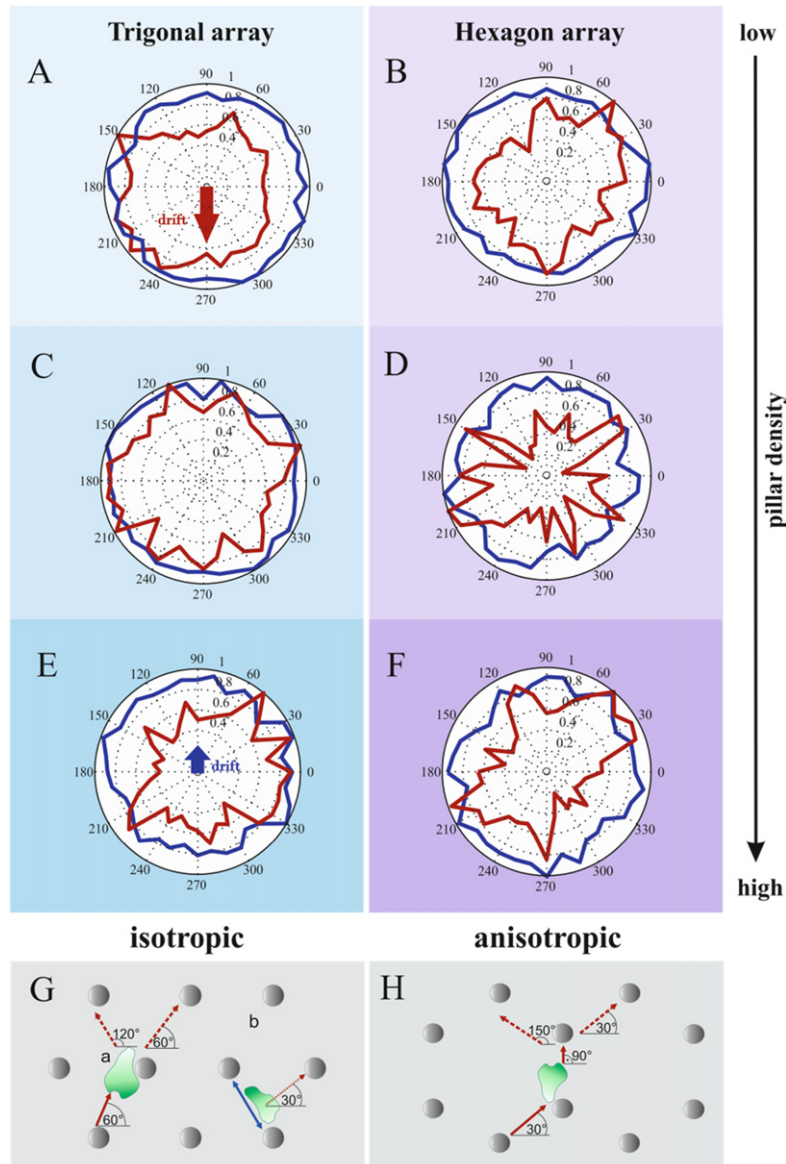


**Figure 4.** Cell migration in pillar lattices of trigonal and hexagonal lattice geometry. Angle distributions of directed (red) and random (blue) cell motion in trigonal versus hexagonal lattices of large (A) (B), intermediate (C) (D) and small (E) (F) inter-pillar distances. Direction of increasing pillar density is indicated by a black arrow. Blue and red arrows indicate directions of long-term (12 h) cell drift along the gradient in inter-pillar distances in trigonal arrays (A), (E). (G) and (H) illustrate the effect of lattice geometry on contact-induced directed runs in trigonal versus hexagonal pillar fields, respectively. Pillars are shown in gray, cells are shown in green, possible directions of contact-induced runs in isotropic trigonal pillar lattices and anisotropic hexagonal lattices are illustrated by arrows. The resulting peaks in the angular distributions are highlighted by way of example for the intermediate density regimes (C) and (D). (G) shows possibilities for cells to either continue a dir-run (a), or to leave a migration-confined rm-state (b) upon sensing a pillar. In the trigonal lattices (a) yields a  $60^\circ$  peak distribution, while (b) adds peaks every  $30^\circ$  (C). (H) illustrates possible way for a cell to perform a succession of dir-runs in a hexagonal lattice, leading to peaks in angular distributions every  $30^\circ$  (D).

In particular, the probability of topographic cell trapping is significantly increased. Further, due to topographic anisotropy in H-arrays, instantaneous velocities of dir-runs exhibit higher values than in T-lattices, indicating a bias in cell migration behavior.

### **Effect of pillar density gradients in trigonal and hexagonal pillar arrays**

The above findings reveal that cell motility states are sensitive to the spatial density and local geometry of the cell environment. We identified different mechanisms how cell migration is influenced by the topographic properties of the pillar lattices. To investigate topographic guidance mechanisms in detail, we analyzed the direction of cell motion as a function of both lattice constant and local geometry of the pillar arrays. Therefore, we compared angular distributions of cell motion during dir-runs and rm-modes in both types of pillar lattices.

#### *Cell guidance by topographic cues*

To investigate topographic guidance of cells induced by the gradient in pillar density, we analyze all migration directions with respect to dir-runs and rm-modes, along (parallel to) the pillar density gradient. As a most important result, our data reveal cell guidance in T-arrays (isotropic lattices) towards regions of intermediate pillar density. This bias of cell migration is governed by dir-run states on the one side, coming from low pillar density regions, and by rm-cell motion on the other side, coming from high pillar density regions. In detail, we find that in trigonal pillar arrays, cells preferably migrate from low density areas (T1) towards more dense (T2) regions (see figure 4(A)) in dir-run mode. Further, we find that during random probing in high density (T3) regions, the migration direction towards intermediate density area is favored (see figure 4(E)). Together, these findings substantiate an overall cell drift to the intermediate density region, which is confirmed by long-term experiments on cell migration in the T-arrays (see last paragraph). We seeded Dd cells ( $N=249$  cells) in trigonal micro-pillar arrays with a gradient in lattice constant and performed spatial distribution statistics of cell positions with respect to the three density regions (T1, T2 and T3) at time points  $t_0=0$  h and  $t_1=12$  h. Before starting the measurement, we waited 20 min to let the cells settle firmly, in order to run the experiment from equilibrium conditions. This way, we minimized convection flows and a possible bias by floating of cells. In order to identify non-biased cell migration behavior, we accordingly kept the experimental setting from any mechanical disturbance during the measurement. At time point  $t_0=0$  h, we find a homogeneous cell distribution over all density regions of the T-arrays. Compared to the time point  $t_0$ , at  $t_1=12$  h the number of cells found in the intermediate pillar density region (T2) increased by 12%, while it decreased by 3% in the low density region (T1) and by 33% in the high density region (T3). To account for cell proliferation during the measurement duration, the acquired cell numbers at time point  $t_1=12$  h are weighted with the proliferation factor of 1.3. Similar long-time experiments in hexagonal pillar lattices with a gradient in pillar density confirm this trend of a net migration of cells towards regions of intermediate pillar density over 12 h. By these results we show that in both trigonal as well as hexagonal lattices with gradients in pillar density, cells tend to invade an intermediate density regime. For longer times, we expect this general trend to progress.

### *Effect of pillar lattice geometry on cell guidance*

In order to investigate mechanisms of the topography-induced cell guidance with respect to the lattice geometry, we analyze the distribution of velocity vector angles of all migrating cells in trigonal and in hexagonal pillar arrays, as shown in figures 4(A)–(F). Please note that, by tilt of the trigonal lattice structure of  $30^\circ$  against the gradient in pillar density, we separate guidance effects along the gradient from guidance effects related to the lattice geometry, i.e. the directions of the lattice vectors. More precisely, the peaks in angular distribution of dir-runs reflect the geometry of the pillar arrays (figures 4(A), (C), (E)), indicating pillar-to-pillar runs in directed migration mode (red).

These peaks originate from the fact that a cell has a significantly increased probability to perform a dir-run upon finding a migration target, i.e. another pillar. In the trigonal pillar lattices, the following mechanisms contribute to the appearance of the peaks. At first, a cell performing a contact-induced pillar-to-pillar run follows a direction along a pillar lattice vector. This mechanism leads to peaks at  $60^\circ$  angles, respectively, as illustrated by cell (a) in sketch principle of figure 4(G). Secondly, if a cell is trapped between several pillars in rm-state, as described above, sensing another pillar can trigger a switch to a dir-run state and to migration leaving the ‘trap’. In this case, the cell starts the run somewhere between the pillars, as illustrated by cell (b) in figure 4(G). In the trigonal array with equilateral triangles the probability for the new migration direction is tilted by  $30^\circ$  against the lattice vectors, thus resulting in peaks at  $30^\circ$  angles, respectively.

For a cell in the hexagonal pillar field, the lattice geometry provides a reduced number of choices for contact-induced runs between next neighbor pillars, compared to trigonal lattices (T-arrays: six options, H-arrays: three options). This results in a distinct  $30^\circ$ -angle distribution of dir-run peaks in H-arrays, as illustrated by figure 4(F). Corresponding to the above explanation, the peaks are most pronounced for angular distributions in intermediate density regions, respectively (figures 4(C) and (D)), showing that for cells performing pillar-to-pillar runs the migration direction is most precise when the inter-pillar distance approximately corresponds to the cell diameter. Moreover, in H-arrays, the reflection of lattice geometry by the angular distribution of dir-runs is more pronounced than in T-arrays (figures 4(B), (D), (F)). This highlights again the effect of the different lattice geometries: in comparison to the isotropic trigonal lattice, in the anisotropic hexagonal array the number of pillars perceived by a cell during dir-runs is lower and thus, the cell polarization and the run towards a target pillar is less disturbed (figures 4(G), (H); see supplementary data movie S2).

In contrast, distinct contact guidance of cells by the pillars is lacking during rm-modes: The angular distributions of random migration phases (blue) in both trigonal and hexagonal arrays do not exhibit a correspondence to lattice geometry (figures 4(A)–(F)). These results are in good agreement with the findings by Arcizet *et al* [31].

## **Conclusions**

In this work we investigate the influence of the quasi-3D environmental topography on cell migration in order to reveal the underlying mechanisms of cell guidance by local topography. For that purpose, two parameters of the quasi-3D environment are systematically varied: the spatial density and the local geometrical structure. In our experiments, we study amoeboid migration of Dd cells within micro-pillar arrays under controlled variation of lattice constant



and lattice geometry. In particular, we compare cell migration in trigonal, isotropic pillar lattices to hexagonal, anisotropic pillar arrays. Based on our observations, we identify general mechanisms governing amoeboid cell migration in quasi-3D environments. We consolidate our findings in a model for the controlled modulation of the two states of amoeboid migration, directed runs and random probing motion.

### **Effect of spatial density on cell motility**

We discriminate cell motion characteristics in three regimes of spatial density with respect to the mean cell size and the cells' radius of sensing. Specifically, the lattice constants range from values close to half the average diameter of a cell to twice the cell size. Our results reveal that spatial density clearly influences amoeboid cell migration modes of directed runs and diffusive-like random probing. Strikingly, directed pillar-to-pillar runs of the cells are facilitated by a high pillar density. This effect is caused by the increased probability for a cell to contact multiple pillars at the same time while performing directed runs, effectively triggering cell polarization. Consolidating this result with the concept of contact-controlled modulation of cell motility, pillars are sensed as attractive topographic stimuli by the cells. In contrast, the random probing motion of cells migrating in arrays of high pillar density shows a diffusive-like character. Here, the mobility is significantly damped by an increasing pillar density, and pillars rather act as obstacles for cell motion. Notably, we find that in a regime where the inter-pillar spacing is in the range of the average cell diameter, cell migration is often confined to small areas in between three and five pillars. As revealed by our analysis, this effect is density-related and results from the geometry of the cell-pillar constellation. Here, the competing attraction by simultaneous pillar contacts inhibits cell polarization that could lead to an escape to the side. Thus, cells are dynamically trapped, moving back and forth between the pillars, without covering large migration distances.

### **Effect of local geometry on amoeboid migration**

To get a detailed view on the specific effect of the local environment geometry on cell migration, we compare cell migration behavior in pillar fields of similar spatial density, but with different lattice structures. Interestingly, we observe distinct changes in the migration behavior upon variation of the pillar lattice geometry: While the density-related effects on cell motility states are analogue in both environments, the absolute values of the migration parameters are strongly affected by the local geometry of the pillar arrays. Significantly, in hexagonal, anisotropic pillar arrays we find a drastic reduction of the overall cell motility. In particular, the probability of a cell to perform a directed run is significantly decreased for the hexagonal pillar arrays. This effect is the result of an increased occurrence of cell trapping in hexagonal lattice geometry, as compared to the trigonal lattices. Due to the modified lattice geometry with the pillar in the center of each hexagon missing, the cells that are in contact with pillars sense fewer topographic attractive stimuli. This lack of topographic attractors prohibits polarization and thus, cell migration to the side. Accordingly, the area probed by cell motion is reduced, even though the hexagonal lattice basically provides the cells with more space due to the missing center pillar. Interestingly, the same geometric condition leads to a more pronounced pillar-to-pillar guidance along the lattice vectors in terms of increased velocity and directional



persistence. This effect is due to the fact that in hexagonal pillar fields, directed cell motion is less disturbed by side attraction.

### **Topographic guidance of amoeboid cell migration**

Our results show that the different topographic influences on amoeboid migration result in guidance of migrating cells. The observed effects reflect the changes in spatial density and local lattice geometry of the pillar fields. In order to investigate the mechanisms of density-gradient guidance, we analyze the angle distributions of the migration directions in trigonal pillar fields with respect to the amoeboid motility modes. By that, we demonstrate that in the low density regime the influence of the local topography on the probability for directed runs is prevalent, leading cells out of these regions towards higher pillar densities. By contrast, in the high density regime, the pillars act as obstacles for the diffusive-like random probing motion. This leads to net shifts of cell positions to lower densities. Consolidating these results, we find that cells tend to invade regions where the inter-pillar spacing is close to the mean cell diameter.

In terms of guidance by the lattice geometry, we show that the angle distributions of the directed run states reflect the directions of the lattice vectors. This effect is more pronounced for the hexagonal lattice, due to the pronounced pillar-to-pillar guidance. In effect, we demonstrate how the analysis of amoeboid cell migration can yield information on the topographic structure of the cell environment, holding interesting perspectives for further investigations.

### **Perspectives**

Our results provide detailed insights into the mechanisms governing amoeboid cell migration in interaction with the topographic structure of 3D environments. We show that cell migration behavior in specific environments can be predicted in detail by the design of quantitative assays. Thoroughly controlled guidance of amoeboid cell migration holds great prospects for medical applications, such as the design of analytical assays for immune cells and smart materials for wound treatment.

Upon transfer of this piloting approach to migration studies of other cell types, the concept is promising for the development of therapeutics and novel materials for regenerative medicine or tissue engineering. In particular, topographic control of mesenchymal cell migration may offer new opportunities for the design of implant materials upon variation of the density and geometrical properties of micron-scaled surface patterns [35].

### **Competing interests**

The authors declare that they have no competing financial interests.

### **Acknowledgements**

The authors acknowledge Dr Delphine Arcizet and Sofia Capito for optimizing the PDMS structure fabrication technique and Dr Delphine Arcizet for the initial version of the I-MSD analysis algorithm (see citations [28, 31]). We thank Dr Günther Gerisch (MPI for Biochemistry, Martinsried, Germany) for providing the Dd cells. DH acknowledges funding

from the Deutsche Forschungsgemeinschaft (grant HE5958-2-1) and Volkswagen-Foundation (grant I85100).

## References

- [1] Evans E 1993 New physical concepts for cell amoeboid migration *Biophys. J.* **64** 1306–22
- [2] Pollard T and Borisy G 2003 Cellular motility driven by assembly and disassembly of actin filaments *Cell* **112** 453–65
- [3] Fisher P, Merkl R and Gerisch G 1989 Quantitative analysis of cell motility and chemotaxis in *Dictyostelium discoideum* by using an image processing system and a novel chemotaxis chamber providing stationary chemical gradients *J. Cell Biol.* **108** 973–84
- [4] Friedl P, Borgmann S and Brockner E-B 2001 Amoeboid leukocyte crawling through extracellular matrix: lessons from the *Dictyostelium* paradigm of cell movement *J. Leukoc. Biol.* **70** 491–509
- [5] Iwadate Y and Yumura S 2008 Actin-based propulsive forces and myosin-II-based contractile forces in migrating dictyostelium cells *J. Cell Sci.* **121** 1314
- [6] Maeda Y, Inose J, Matsuo M, Iwaya S and Sano M 2008 Ordered patterns of cell shape and orientational correlation during spontaneous cell migration *PLoS ONE* **3** e3734
- [7] Li L, Nørrelykke S F and Cox E C 2008 Persistent cell motion in the absence of external signals: a search strategy for eukaryotic cells *PLoS ONE* **3** e2093
- [8] Benichou O, Loverdo C, Moreau M and Voituriez R 2006 Two-dimensional intermittent search processes: An alternative to Lévy flight strategies *Phys. Rev. E* **74** 020102
- [9] Dalous J *et al* 2008 Reversal of cell polarity and actin–myosin cytoskeleton reorganization under mechanical and chemical stimulation *Biophys. J.* **94** 1063–74
- [10] Friedl P 2004 Prespecification and plasticity: shifting mechanisms of cell migration *Curr. Opin. Cell Biol.* **16** 14–23
- [11] Devreotes P and Zigmond S 1988 Chemotaxis in eukaryotic cells: a focus on leukocytes and dictyostelium *Annu. Rev. Cell Biol.* **4** 649–86
- [12] Ridley A *et al* 2003 Cell migration: integrating signals from front to back *Science* **302** 1704–9
- [13] Parent C and Devreotes P 1999 A cell's sense of direction *Science* **284** 765–70
- [14] Manahan C, Iglesias P, Long Y and Devreotes P 2004 Chemoattractant signaling in *Dictyostelium discoideum* *Annu. Rev. Cell Dev. Biol.* **20** 223–53
- [15] Jeon N *et al* 2002 Neutrophil chemotaxis in linear and complex gradients of interleukin-8 formed in a microfabricated device *Nat. Biotechnol.* **20** 826–30
- [16] Irimia D *et al* 2006 Microfluidic system for measuring neutrophil migratory responses to fast switches of chemical gradients *Lab Chip* **6** 191–8
- [17] Song L *et al* 2006 *Dictyostelium discoideum* chemotaxis: threshold for directed motion *Eur. J. Cell Biol.* **85** 981–9
- [18] Meier B, Zielinski A, Weber C, Arcizet D, Youssef S, Franosch T, Rädler J O and Heinrich D 2011 Chemical cell trapping in controlled alternating gradient fields *Proc. Natl Acad. Sci.* **108** 11417–22
- [19] Verkhovskiy A, Svitkina T and Borisy G 1999 Selfpolarization and directional motility of cytoplasm *Curr. Biol.* **9** 11–20
- [20] Lo C, Wang H, Dembo M and Wang Y 2000 Cell movement is guided by the rigidity of the substrate *Biophys. J.* **79** 144–52
- [21] Saez A, Ghibaudo M, Buguin A, Silberzan P and Ladoux B 2007 Rigidity-driven growth and migration of epithelial cells on microstructured anisotropic substrates *Proc. Natl Acad. Sci.* **104** 8281
- [22] Kemkemer R, Neidlinger-Wilke C, Claes L and Gruler H 1999 Cell orientation induced by extracellular signals *Cell Biochem. Biophys.* **30** 167–92

- [23] Kemkemer R, Jungbauer S, Kaufmann D and Gruler H 2006 Cell orientation by a microgrooved substrate can be predicted by automatic control theory *Biophys. J.* **90** 4701–11
- [24] Kaiser J, Reinmann A and Bruinink A 2006 The effect of topographic characteristics on cell migration velocity *Biomaterials* **27** 5230–41
- [25] Frey M, Tsai I, Russell T, Hanks S and Wang Y 2006 Cellular responses to substrate topography: role of myosin II and focal adhesion kinase *Biophys. J.* **90** 3774–82
- [26] Tan J, Shen H and Saltzman W 2001 Micron-scale positioning of features influences the rate of polymorphonuclear leukocyte migration *Biophys. J.* **81** 2569–79
- [27] Tan J, Shen H, Carter K and Saltzman W 2000 Controlling human polymorphonuclear leukocytes motility using microfabrication technology *J. Biomed. Mater. Res.* **51** 694–702
- [28] Arcizet D, Meier B, Sackmann E, Rädler J and Heinrich D 2008 Temporal analysis of active and passive transport in living cells *Phys. Rev. Lett.* **101** 24
- [29] Steinberg T *et al* 2007 Early keratinocyte differentiation on micropillar interfaces *Nano Lett.* **7** 287–94
- [30] Simon Y, Sebastian G and Joachim O R 2011 Automated tracking in live-cell time-lapse movies *Integr. Biol.* **3** 1095–101
- [31] Arcizet D, Capito S, Gorelashvili U M, Leonhardt C, Vollmer M, Youssef S, Rappl S and Heinrich D 2012 Contact-controlled amoeboid motility induces dynamic cell trapping in 3D-microstructured surfaces *Soft Matter* **8** 1473–81
- [32] Palchesko R N, Zhang L, Sun Y and Feinberg A W 2012 Development of polydimethylsiloxane substrates with tunable elastic modulus to study cell mechanobiology in muscle and nerve *PlosOne* **7** 1–13
- [33] Ladam G, Vonna L and Sackmann E 2005 Protrusion force transmission of amoeboid cells crawling on soft biological tissue *Acta Biomater.* **1** 485–97
- [34] Delanoë-Ayari H, Rieu J P and Sano M 2010 4D traction force microscopy reveals asymmetric cortical forces in migrating dictyostelium cells *Phys. Rev. Lett.* **105** 248103
- [35] Le Berre M, Liu Y-J, Hu J, Maiuri P, Bénichou O, Voituriez R, Chen Y and Piel M 2013 Geometric friction directs cell migration *Phys. Rev. Lett.* **111** 198101